Study and Application of Electrochemical Impedance Spectroscopy for Quickly Evaluating the Performance of Coatings and Predicting the Failure Time in the Development of Waterborne Epoxy Micaceous Iron Oxide Coatings

Zhonghua Chen[1,2], Chang He[1,], Fei Yu[1**], Yi Wang[1]*

[1] College of Material Science and Engineering, South China University of Technology, Guangzhou 510640, China
[2] Guangzhou Jointas Chemical Co. Ltd., Guangzhou 510530, China
[*]E-mail: hechscut@163.com
[**]Email: flyb1999@gmail.com

The possibility and necessity of using electrochemical tests to characterize the coating performance and guide the development and application of coating products were discussed. An attempt was made to establish the relationship between the electrochemical parameters and the macroscopic behavior of the coating. Waterborne micaceous iron oxide epoxy coatings were prepared and characterized by SEM, Electrochemical Impedance Spectroscopy (EIS) and conventional corrosion tests. The effects of the particle size and the pigment volume concentration (PVC) on the corrosion properties were discussed. Results revealed that the good anticorrosive performance of the paint was obtained when the 600-mesh-sized MIO was used and the pigment volume concentration (PVC) was 39%. The consistency of the two EIS parameters (the partial fitting coating resistance R_{part} and the phase angle at 10 Hz) for evaluating the performance of the coatings was confirmed. The electrochemical failure time (EFT) was defined, and then compared with the macroscopic blistering time, which verified the possibility of applying this parameter in the development of coating products.

1. INTRODUCTION

Theoretical studies on the degradation and failure mechanisms of coatings and lifetime prediction of anticorrosive coatings by EIS have been carried out for many years [1-4]. In these studies, the equivalent electrical circuit (EEC) is often used to obtain electrochemical parameters and

then the performance of coatings is analyzed. But in fact, the equivalent circuit requires a lot of experience to be established due to the uncertainty of the equivalent circuit, and it is also time-consuming [5]. Researchers proposed the use of raw data, instead of the complicated fitting parameters, to evaluate the coatings studied [5-14]. Y. Zuo et al [15] proposed the phase angle at 10 Hz to reflect the performance of coatings, because the variation of $\boldsymbol{\phi}_{10Hz}$ is more identical with the change of coating resistance. L. Liang et al [16] proposed the partially fitted coating resistance from high-frequency EIS data to evaluate the protectiveness of coatings. These parameters can show the anticorrosion performance of the anticorrosive coating, which are collected in the middle and high frequency ranges. However, whether there exist associations or consistencies among these characteristic parameters hasn't been studied yet. The effectiveness of these methods for evaluating the performance of the coatings studied needs to be tested. Meanwhile, the relationship between the electrochemical parameters and conventional corrosion tests also needs to be discussed, in an attempt to accelerate the testing of the anticorrosion performance and guide the development of the coating products.

Micaceous iron oxide epoxy coating is usually used in the field of heavy-duty coatings, and the coatings primarily act as physical barrier to extend the time it takes for the corrosive medium to penetrate into the primer and the substrate. Different from that in the oil paint, the MIO with larger density is difficult to be dispersed and stable in the water-based paint. So the particle size of the natural MIO has a significant impact on the dispersion in the waterborne system, thereby affecting the anticorrosion properties of the coatings [17]. P. Kalenda et al [18] studied the effect of lamellar pigments concentration (expressed as PVC) on the anticorrosion properties. Similarly, the content of MIO has a significant effect on the corrosion resistance of the epoxy coatings [19].

In this paper, waterborne micaceous iron oxide epoxy coatings were prepared. Simultaneously, conventional corrosion tests and EIS were used to characterize the anticorrosion properties of the coatings. The failure behavior of the waterborne micaceous iron oxide epoxy coating system was studied. And two different methods were applied to evaluate the performance of coatings. Then, the relationship between the macroscopic state of the coating and the electrochemical parameters was analyzed, which may help to quickly evaluate the coating performance and accelerate the development of coating products.

2. EXPERIMENTAL

2.1 Materials

Waterborne epoxy resin EP 5230 and curing agent EK 8545 were produced by Hexion Specialty Chemicals (America). EP 5230 is high-molecular weight solid epoxy dispersion, of which the solid content is 55%. Its epoxy equivalent is about 500 g/mol, the epoxy index about 2 mol /kg, the molecular weight about 1000, the density 1.20 g/ml and the viscosity of the epoxy resin about 10 000 Pa·s at 25 ℃. EK 8545 is waterborne modified amine adduct, and its amine value (mg of KOH) is 260 mg/g, the solid content 52%.

The MIO is derived from natural mirror iron ore, produced in Anhui, China. Its main component is α-Fe$_2$O$_3$. The iron content, expressed as Fe$_2$O$_3$, is not less than 93%. Its oil absorption value is 13%, the residue on sieve (63 μm) not more than 1% and the content of silica not more than 3.0%. The content of flake mica iron oxide reaches about 60%. Fig. 1 presents MIO of different particle size. Obviously, The MIO of 600 mesh shows a greater ratio of thickness to diameter.
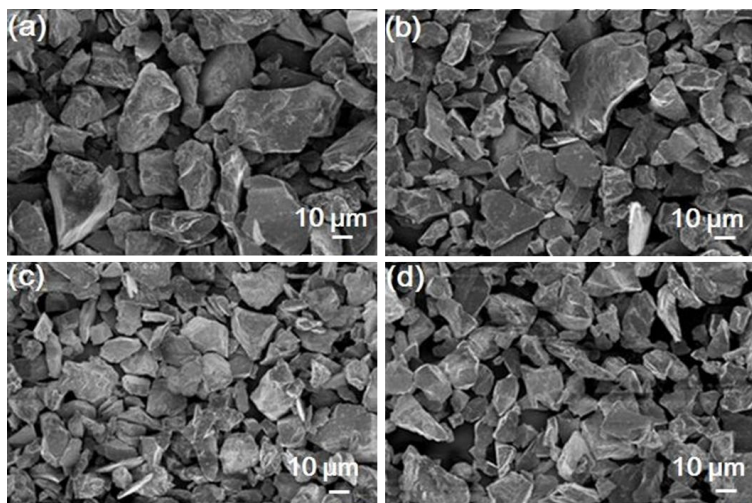
Figure 1. SEM micro morphologies of the MIO of different particle size: (a) 325 mesh, (b) 400 mesh, (c) 600 mesh, (d) 800 mesh.

2.2 Characterization

The morphologies of MIO were characterized by NOVA NANOSEM 430 scanning electron microscopy (SEM) (FEI Corporation, Holland). The fractured surfaces of coatings with different PVC were also characterized by NOVA NANOSEM 430. The morphologies of the rust were characterized by NOVA NANOSEM 430 and ZC-XW-07 optics microscope (China).

2.3 Preparation of coatings

Waterborne epoxy resin and waterborne coating additives (such as dispersing agent, antifoaming agents, corrosion inhibitor and so on) were added into water with moderate-speed stirring for 15 min. Then the MIO pigment was added and mixed at high-speed stirring for about 45 min until the fineness of coatings was lower than 60 microns. Other additives such as leveling agent, antifoaming agent and rheological agent were added with stirring mildly for 15 min. The component A of waterborne epoxy micaceous iron oxide paint was obtained. Note that the choice of MIO was shown in Table 1, and the PVC was shown in Table 2. The component B was the waterborne curing agent.

When preparing the samples, the component A and B were homogeneously mixed in a weight ratio of 10:1 (the weight ratio of the resin and the curing agent was 3.6:1).

2.4 Testing of coatings

The system studied consisted of polished carbon steel, coated with coatings prepared. The steel plate was carefully polished with silicon carbide abrasive paper after preliminary clean with acetone, and finally cleaned thoroughly with acetone. The system studied was dried for 7 days under normal temperature and humidity environments (temperature: 25 ℃, humidity: 50%). The thickness of the films was measured by an electromagnetic thickness gauge. The accuracy of the gauge was ±3% of the reading. Sample 1~8 were prepared (as shown in Table 1 and Table 2), of which the thickness was 100±5 μm.

In the accelerated test, carbon steels with a nominal thickness of 0.8 mm coated samples were immersed in sodium chloride solution (3.5 wt%) according to ASTM D 543-67, and exposed to neutral salt spray chamber (5 wt% sodium chloride solution) in accordance with ASTM B117. The temperature of the salt spray chamber was 35±3 ℃. The adhesion test was in accordance with ASTM D 3359-93. For each sample three parallel experiments were performed.

2.5 Electrochemical Impedance Spectroscopy (EIS)

The EIS measurements were carried out with PGSTAT2273 electrochemical workstation. The three-electrode cell for EIS included a standard calomel reference electrode, a steel plate counter electrode of 4.5 cm^2 in area, and a working electrode (carbon steels coated samples) of 15 cm^2 in area, immersed in 3.5 wt% sodium chloride solution, and the EIS measurement were performed at room temperature(25 ℃) in a faraday shielding box. The shielding device does not isolate the test device from the air, but shields against the external interference to the test. The measurement frequency ranged from 100 kHz to 10 mHz, using a sinusoidal potential perturbation of 10 mV amplitude.

After a period of exposure, the performance of coatings was evaluated by EIS measurements and visual assessment. At the initial stage, samples were evaluated and observed every 4 hours, after then, every 12 hours. Three parallel experiments were performed in each experiment to ensure reproducibility. The data were analyzed by ZSimpWin software. The tolerance of the fitting data was usually below 5%.

3. RESULTS AND DISCUSSION

3.1 Influences of the particle size of MIO on the protection performances of coatings

MIO acts as a barrier in waterborne epoxy micaceous iron oxide paint, which reduces the corrosive species transport through the film. MIO with proper particle size (as shown in Fig. 1) can effectively improve the shielding properties of the coatings, which was called "labyrinth effect".

Table 1 presents the results of the first four coating samples (from sample 1 to sample 4) exposed in the 3.5 wt% sodium chloride solution and in the salt spray chamber. When the particle size of MIO is 600 mesh, the blistering time of coatings in sodium chloride solution test (SCST) reaches

400 h, and the ranking of coatings in neutral salt spray test (NSST) is the lowest. As is shown in Fig. 1, the MIO of 600 mesh has larger ratio of diameter to thickness than others. However, some of the MIO of 325 mesh or 400 mesh have lower ratios of thickness to diameter and coarse particle, resulting in precipitation. The particle of 800 mesh has a lower particle size and less flake structure. Additionally, some of them show a long strip structure. These factors may lead to the poor "labyrinth effect".

Table 1. Sample 1-4 and their result of conventional corrosion tests.

Samples	Average particle size / mesh	Adhesive/level	Blistering time of coatings in SCST/ h	Ranking of coatings in NSST (exposed 25 d)
Sample 1	325	1	285	4
Sample 2	400	1	275	4
Sample 3	600	1	400	2
Sample 4	800	1	350	3

Note: the ranking of coatings is in according to ISO 4628-2-2003.
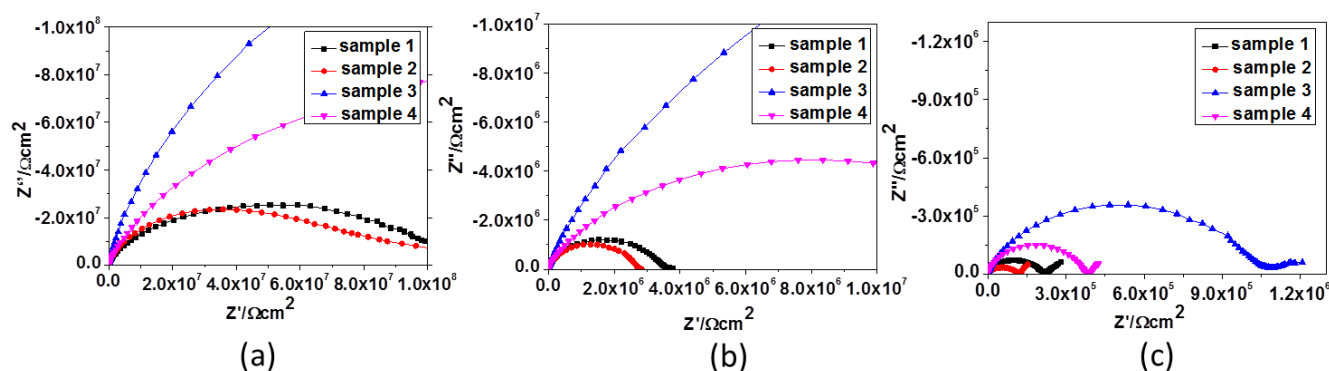
Figure 2. Nyquist plots for sample 1-4 at three different immersion times: (a) 0 h, (b) 24 h, (c) 360 h.

Fig. 2 shows impedance spectra of sample 1-4 in the different immersion time. From Fig. 2(a) and (b), there has only one capacitive arc in the impedance diagrams. In addition, sample 3 shows the largest impedance loop in the high frequency, which is attributed to the excellent anti-permeability of the coatings. After 360 h of immersion, dramatic changes take place in electrochemical impedance. The four samples respectively exhibit an extra new arc in the low-frequency region because of finite length diffusion. But sample 3 reveals one larger impedance arc in the high frequency region, which reflects the property of the coating. The analyses above show that the particle size of MIO has a significant impact on the protection performance of the coatings. Due to the appropriate particle size of the MIO with 600 mesh and its higher content of the flake particles, sample 3 exhibits better barrier properties, delaying the penetration of the corrosive media into the substrate surface and postponing the occurrence of corrosion reactions, which reflects the slow decrease of the impedance arc and the delayed emergence of the diffusion arc in the low-frequency region on the Nyquist diagram [11, 21].

It should be emphasized here that different anti-corrosion mechanisms exhibit different variations of capacitive arc. For example, the anti-corrosion mechanism of zinc-rich paint is sacrificial-to-barrier protection. The zine-rich paints may exhibit low value of impedance modulus in the early immersion [14]. After immersion for a short time, two time constants appear rapidly in the impedance spectroscopy of zine-rich coating and the coating resistances of zine-rich coatings may increase because of the sacrificial protection [3].

3.2 Effect of pigment volume concentration (PVC) on the performances of coatings

Table 2. Effect of different PVC on the performances of coatings.

Samples	PVC/%	Adhesive/level	Blistering time of coatings in SCST/ h	Ranking of coatings in NSST(exposed 30 d)
Sample 5	54	1	137	4
Sample 6	47	1	200	4
Sample 7	39	0	550	1
Sample 8	30	0	390	2

Note: the mesh-size of MIO for samples 5-8 is 600 mesh.
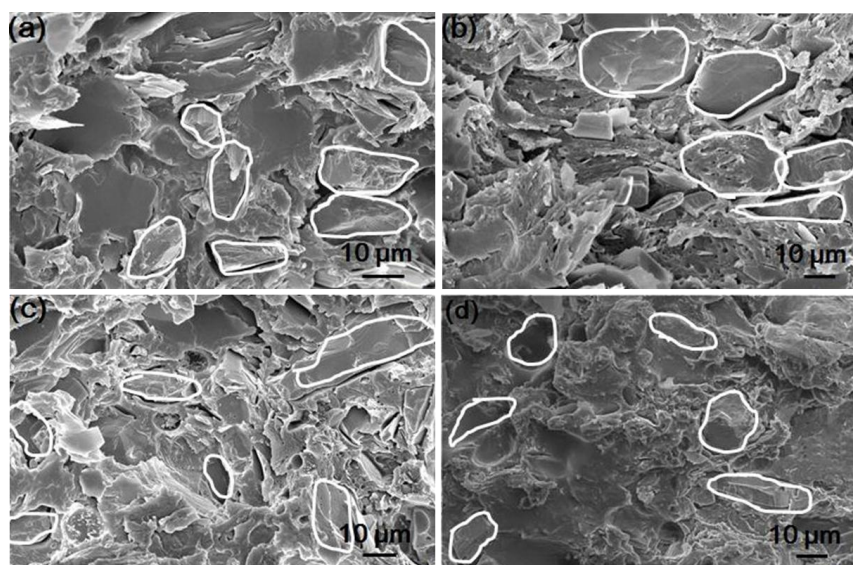
Figure 3. SEM micro morphology of sample 5-8 with different PVC.

PVC has a great influence on corrosion resistance of the coating [20]. For the protective coatings with shielding mechanisms, the PVC affects the labyrinth effect through changing the relationship between the resin and pigments. As is shown in Table 2 and Fig. 3, when the PVC of coatings is high, the MIO unevenly disperses in the coatings systems, forming a local accumulation and a large number of pores. These defects may provide a good channel for the rapid penetration of the electrolyte into coating body, so the durability of the protective film in SCST is poor and the ranking of coatings in NSST is also lower. From the figure, with the decrease of PVC from 54% to 39%, the

proportion of resin increased, and the dispersity of the pigment in coating body is improved, resulting in reduction of the number of pores. When the PVC is 39%, the pigment is evenly dispersed in the resin. And the flake pigments orientation tends to be slightly parallel to each other. So the durability of the protective film in SCST increases and the ranking of coatings in NSST also increased. As the PVC reduces to less than 39%, the low content of flake pigments results in weak labyrinth effect, which means that the barrier of the film on the substrate is reduced.
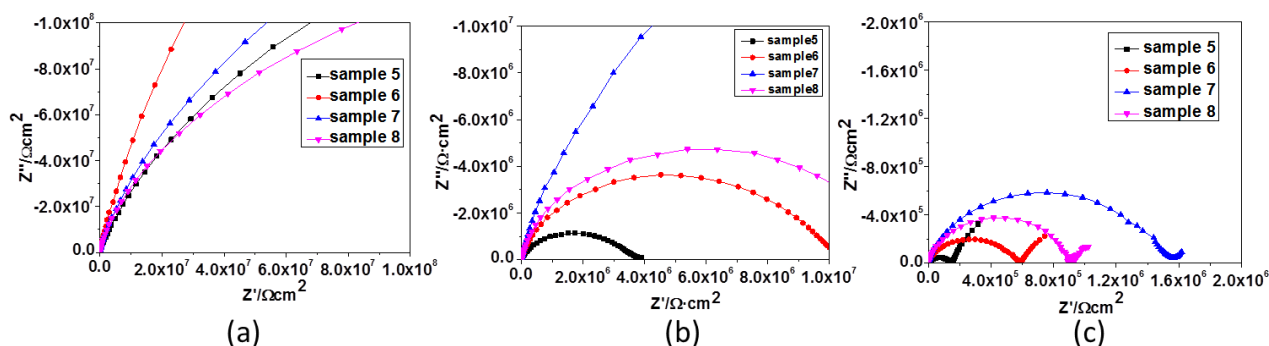

Figure 4. Nyquist plots for samples 5-8 at three different immersion times: (a) 0 h, (b) 24 h, (c) 360 h.

Fig. 4 shows the electrochemical impedance spectra of sample 5-8 at different immersion times. The Nyquist diagrams shown in Fig. 4(a) display that these 4 samples have only one typical capacitive arc in the complex plane, respectively, and the coating resistance remained above 10^8 $\Omega \cdot cm^2$ before immersion. The Nyquist diagrams shown in Fig. 4(b) also exhibit one capacitive arc in the complex plane of samples 5- 8 after an immersion time of 24 h. Sample 7 shows a larger capacitive arc. Fig. 4 (c) displays two apparent capacitive arcs in the complex plane of sample 5-8 after an immersion time of 360 h. As can be seen from the analysis below, the capacitive arcs in the low frequency region represent the diffusion of corrosion products. And simultaneously, sample 7 shows a smaller arc at the low frequency region, which suggested the diffusion of corrosion products is weakened and the corrosion degree of the substrate is the lowest. From the discussion above, sample 7 (PVC is 39%) provides a better barrier to protect the coatings.

3.3 Evaluation of methods for quickly predicting the performances of coatings

Fig. 5 shows typical sets of EIS data of the studied coatings at different exposure times in SCST. At the early immersion stage, the coatings studied exhibit a lager capacitive arc in the Nyquist plots, of which the dielectric response shows properties of the coating. Its EEC is shown in Fig. 6(a). The coating serves as a barrier layer, and the coating resistance (R_{coat}) is very large. After a few hours of immersion, we found the EEC (Fig. 6a) cannot fit the data properly, especially in the middle and low frequency regions. It could be seen from the impedance spectroscopy that using the model b in Fig. 6 can fit well. This indicates that the electrolyte solution arrives at coating/steel interface, and the corrosion reaction takes place at the coating/steel interface. At this stage, the impedance spectroscopy

shows only one gradually reduced capacitive arc, indicating continuous penetration of the electrolyte solution and slight electrochemical reactions. Meanwhile, the macroscopic appearance of the coating is intact as well. With the immersion time increasing, a diffusion tail appears in the impedance spectroscopy due to the fact that the mass transfer process of corrosion product is hampered in the presence of mica iron oxide pigments [21]. Its EEC is shown in Fig. 6(c). The low-frequency diffusion arc gradually evolved into a similar diffusion straight line over time, which is often accompanied by the generation of macroscopic blisters in the coating surface. And then the test is terminated, because a long-time test conducted till the coatings completely fall off from the substrate does not comply with test specification.
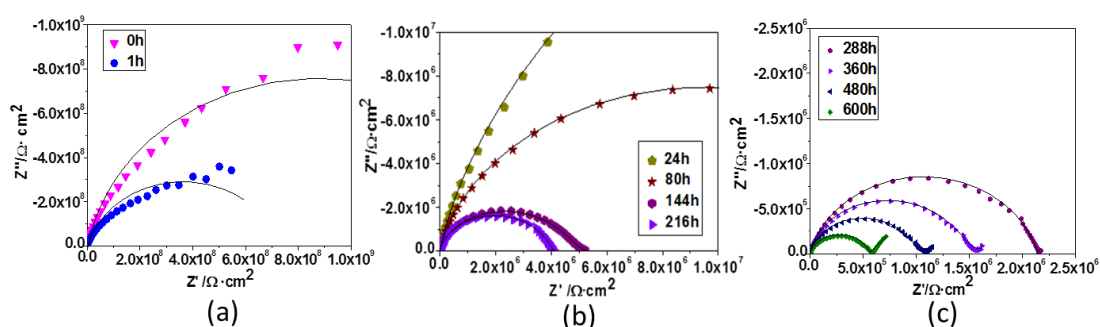
Figure 5. Typical Nyquist diagrams of sample 7 at different immersion times. (a)-(c) represent the three different stages of the impedance spectrum:(a) 0-1 h, (b) 24-216 h, (c) 288-600 h.
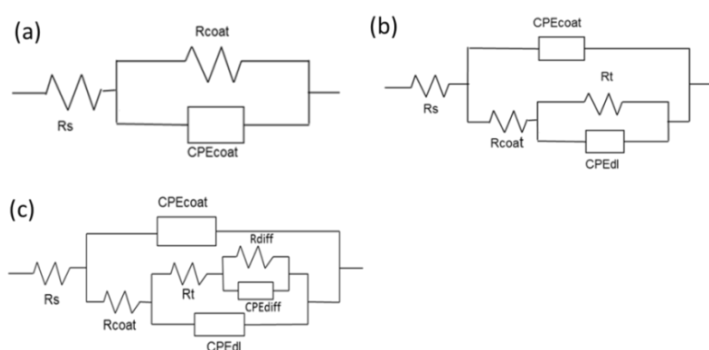
Figure 6. EECs used to fit EIS diagrams of coatings in during immersion time. R_s is the solution resistance. R_{coat} is the coating capacitance. CPE_{coat} is the coating capacitance. R_t represents charge-transfer resistance and CPE_{dl} represents double- layer capacitance. R_{diff} and CPE_{diff} shows diffusion resistance and the mass transfer process of diffusates, respectively.

In this section, the anticorrosion performance of the coating samples is quickly evaluated by the phase angle of 10 Hz ($\boldsymbol{\phi}_{10Hz}$) and the partial fitting coating resistance (R_{part}) method, respectively. Table 3 shows the coating resistance of samples 5-8 with different immersion time in SCST.

Table 3. Coating resistance (R_{coat}) with immersion time in SCST.

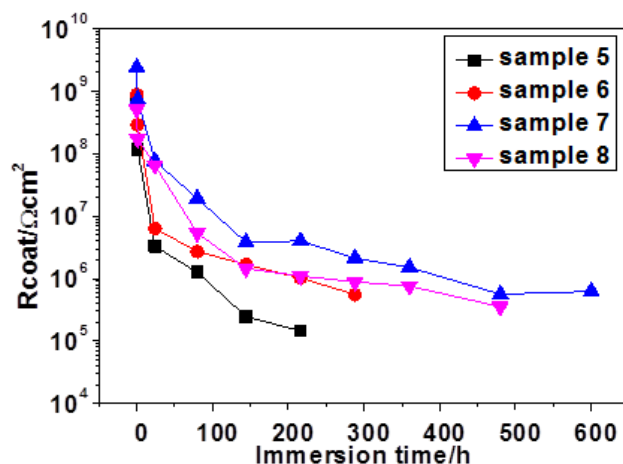|	Coating resistance, $R_{coat} \times 10^6/\Omega cm^2$									
Time/h	0	1	24	80	144	216	288	360	480	600
Sample 5	745±31.3	116±2.28	3.28±0.15	1.26±0.016	0.24±0.01	0.15±0.004	-	-	-	
Sample 6	882±34.5	289±6.13	6.30±0.25	2.73±0.07	1.69±0.048	0.93±0.04	0.65±0.02	-	-	
Sample7	2374±93.5	736.3±11.1	75.9±2.3	19.25±0.86	3.81±0.11	4.01±0.16	2.13±0.08	1.51±0.05	0.56±0.02	0.62±0.02
Sample 8	515±21.3	170±4.62	11.2±0.38	5.37±0.37	1.41±0.034	1.11±0.03	0.89±0.036	0.75±0.03	0.35±0.01	

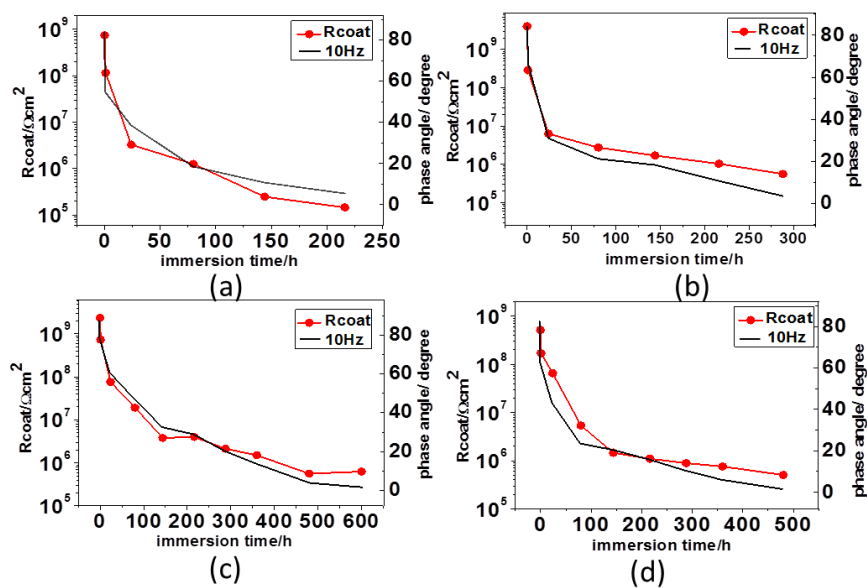**Figure 7.** The variations of the coatings resistance with immersion time for samples 5-8.

Fig. 7 shows the variations of coating resistance (R_{coat}) with immersion time for sample 5-8. The figure shows that R_{coat} decreases rapidly in the early, followed by a slow decrease. The coating resistance is related to the porosity of the coating. In the early stage of immersion, the electrolyte solution penetrates into the coating body at a higher initial rate, resulting in rapid increase of porosity, followed by a slow rise of porosity due to the blocking of inert pigments and the presence of diffusion medium. When R_{coat} decreases to about $1.0 \times 10^6 \, \Omega \cdot cm^2$, a significant capacitance tail or arc appears in Nyquist diagrams at low frequency region, which indicates the electrochemical corrosion reactions of the steel substrate underneath have already strongly occurred, but no visible blisters at that moment. At this time, it is generally considered that the protective performance of the coatings is poor. The experimental results also show that when the coating resistance decreased to the range between 10^5 $\Omega \cdot cm^2$ and $10^6 \, \Omega \cdot cm^2$, a small amount of macroscopic blisters began to appear in the coating surface.

Fig. 8 displays variations of R_{coat} and R_{part} of sample 5-8 with immersion time. The results show that the trends of R_{part} with time are almost similar to that of R_{coat} fitted from all data, especially during this period from immersion for 24 h to the coating beginning to blister. It shows that R_{part} can be applied to evaluate anticorrosion properties of such coatings, which is expected to avoid time-consuming impedance test at the low frequency. In the slow decrease stage, when the resistances of the coating are close to $10^6 \, \Omega \cdot cm^2$, the partial fitting coatings resistances are also close to $10^6 \, \Omega \cdot cm^2$. At this time, it is considered that the electrochemical reaction has strongly occurred at the steel/coating

interface, despite of the good appearance of the coating. Sample 7 shows the maximum coating resistance and more durable protection for the substrate.
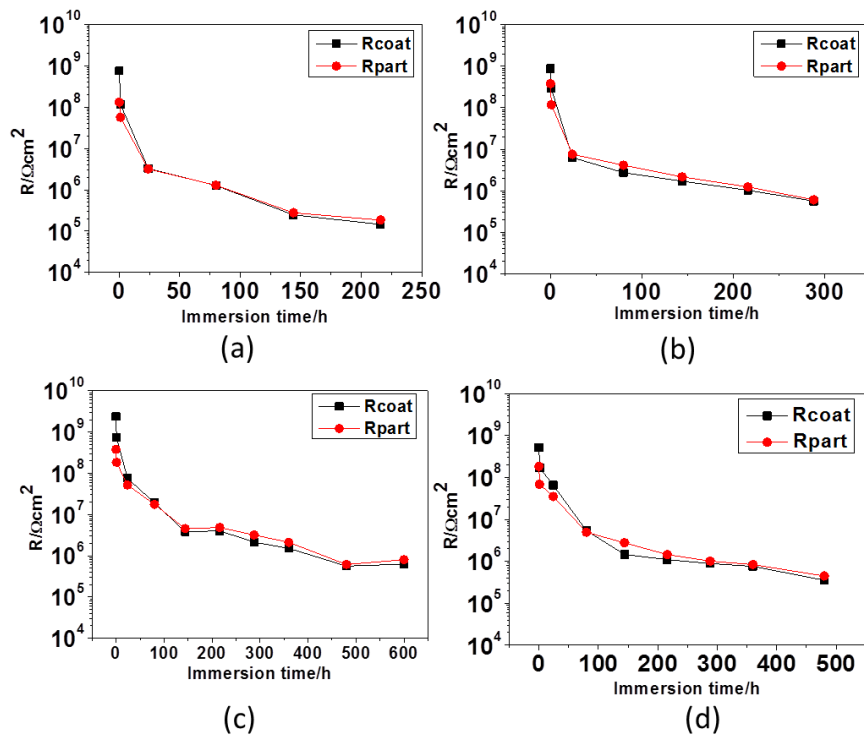
Figure 8. The variations of R_{coat} and R_{part} with immersion time for (a) sample 5, (b) sample 6, (c) sample 7, and (d) sample 8. R_{coat} is fitted from all data (100 kHz to 0.01 Hz); R_{part} is fitted from 100 kHz to 10 Hz.

Figure 9. The variations of R_{coat} and ϕ_{10Hz} with immersion time for (a) sample 5, (b) sample 6, (c) sample 7, and (d) sample 8.

Fig. 9 represents variations of R_{coat} and $\boldsymbol{\phi}_{10Hz}$ of samples 5-8 with immersion time for sample 5-8. The phase angle is based on the following form:

$$\phi = \arctan(-Z''/Z') = \arctan(\omega R_c C_c)$$

ω is the current frequency. R_c represents the coating resistance, and C_c is coating capacitance. In the early stages, the coating is more intact, resulting in the R_c large and C_c very small. And the changing rate of R_c is verified to be much higher than that of C_c [11], resulting in that the changes of the coating resistance and the phase angle at a given frequency is similar. However, the changing rate of C_c cannot be negligible later. But in this stage before the coating fails seriously, the trend of both still tend to be similar, as shown in Fig. 9. From Fig. 9, after immerse for some time, R_{coat} of sample 5-8 decrease to about 10^6 $\Omega \cdot cm^2$, and the $\boldsymbol{\phi}_{10Hz}$ decreases to the range between 10° and 20°, indicating the effect of the electrochemical reaction under the coatings.

EIS and SCST show that in the early stage, the electrolyte penetrates into the coating, resulting in a rapid decrease in R_{coat}. In the second stage, the coating resistance decreases slowly. According to the EEC, electrochemical reaction has taken place, but there is still only one capacitive arc in the impedance spectrum. When a diffusion tail or arc starts to be showed in the impedance spectrum, the R_{coat} is near 10^6 $\Omega \cdot cm^2$, and the R_{part} and $\boldsymbol{\phi}_{10Hz}$ is close to 10^6 Ωcm^2 and the range of 10°-20°, respectively. There exists diffusion resistance of corrosion product in the coating body due to the barrier of the flake pigment. Although the appearance of the coating is in good condition, the coating is considered to have electrochemically failed. In the last stage, the apparent diffusion arc or straight line shows in the impedance spectrum. Meanwhile, the coating resistance decreases to the range between 10^5 Ωcm^2 and 10^6 Ωcm^2, and the phase angle at 10 Hz reaches the range between 0 ℃ and 10 ℃. The corrosion reaction is substantially more serious. At this time, the coating surface starts to blister, indicating macroscopic failure. The two different methods for rapidly evaluating the properties of coatings are proved to be consistent, which demonstrated their effectiveness for evaluating the properties of coatings and advantage to the development and application of coating products.

3.4 Comparison of electrochemistry failure time and macroscopic defects of the film

The appearance of a small capacitive tail or arc at the low frequency suggests the confessed damage to protective properties of coating. The EFT is defined as the time of the appearance of a small capacitive tail or arc in this experiment. Table 4 shows the EFT of sample 1-8. Comparison of the EFT and macroscopic blistering time is shown in Fig. 10. As is shown in Fig. 10(a) and (b), with the reduction of the particle size of MIO for sample 1-4, these three parameters, including EFT, blistering time in SCST and ranking of coating in NSST, first increase and then decline. As discussed above, when the particle size of MIO is 600 mesh, this coating (sample 3) has a better barrier effect on the substrate, thus the anticorrosive performance improves and the EFT becomes longer. Due to the low content of the 800-mesh-sized MIO with flake structure, the anticorrosion properties of sample 8 is weak and the EFT is shortened. The samples 5-8 represent a similar law of the three parameters as shown in Fig. 10(c) and (d). It proves that sample 7 shows the best anticorrosion properties in the conventional corrosion test and EIS test.

Table 4. the electrochemistry failure time of sample 1-8.

samples	Sample 1	Sample 2	Sample 3	Sample 4	Sample 5	Sample 6	Sample 7	Sample 8
the EFT/h	196	164	310	227	80	105	270	180
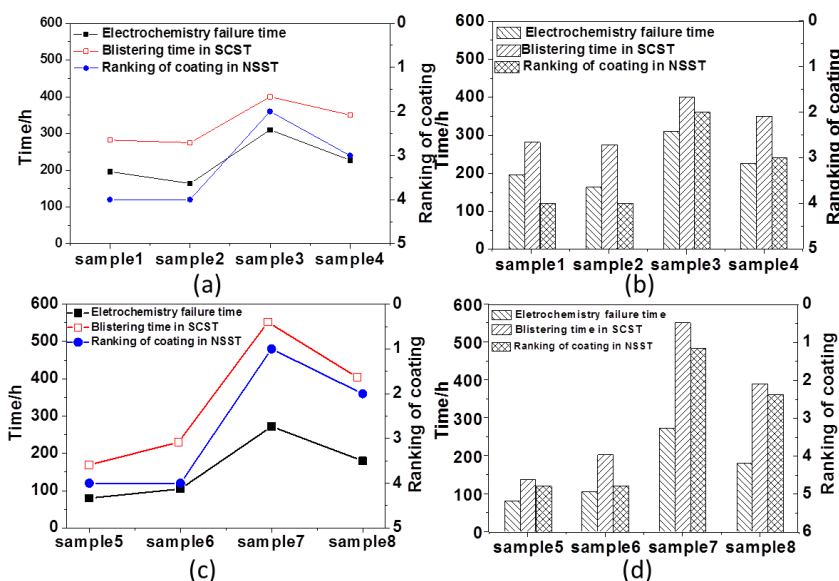
Figure 10. Comparison of the EFT and macroscopic blistering. The figure respectively shows the electrochemical failure time, blistering time in SCST and the ranking of coatings in NSST.

Experiments show that the EFT does not correspond to the appearance of macroscopic defects on the coatings surface. After the electrolyte solution reaches the coating/steel interface and the strong corrosion electrochemical reaction occurs, the adhesion between the coating and the substrate is gradually weakened and the surface exhibits macroscopic blisters finally [22-23]. For example, the morphologies of blisters on the coating surface of sample 7 are shown in Fig. 11.

As is shown in Fig. 11(a1), after a long period of NSST, there accumulates some rust under some blisters, and it is bright bare metal substrate under other blisters. With the corrosion reaction progressing, the rust accumulates in a large amount, producing the expansion of the volume, thereby the coating surface blisters [24]. The shape of these blisters is different, including circular and irregular shape. The micro morphology of the rust is shown in Fig. 11(b1) and (b2), indicating the presence of two or more corrosion reaction mechanisms [25]. Meanwhile, as shown in Fig. 11(a2) and (a3), there is almost no rust under blisters. Currently, there is no unified blistering mechanism to account for the all blistering phenomenon. The osmotic pressure and the internal stress are generally considered to be major causes of blistering in neutral aqueous solutions [25, 26], which can explain why the steel under the blisters are smooth [27]. However, the essence of the two blistering situations is that the adhesion between the coating and the substrate is weakened by other external force.
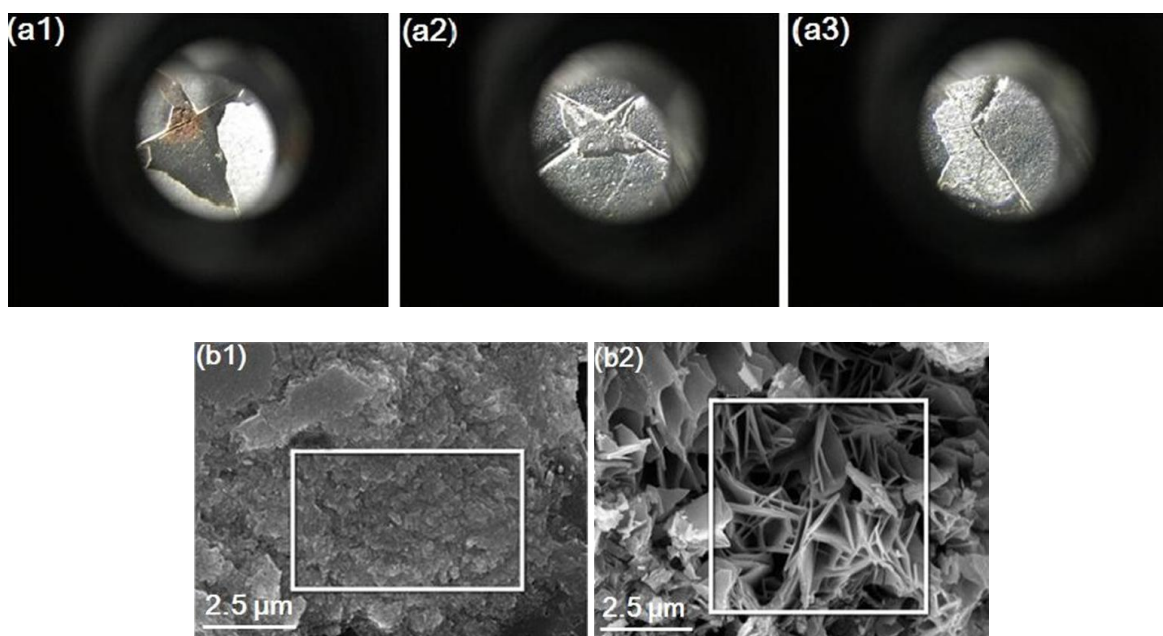
Figure 11. (a) Optical photos of blisters on the coating surface of sample 7: (a1) and (a2) in NSST; (a3) in SCST; (b) SEM micro morphologies of the rust in the coating/steel interface of sample 7.

The EFT is often less than the time to generate macro-defects, where there is a time interval. The time interval is significantly important for shortening the time of conventional corrosion tests. From Fig. 10, the maximum time interval reduced by about 50%. According to the mechanism analysis of blistering, the adhesion of the coatings has a significant correlation with blistering. Improving the adhesion of coating can enhance the ability to resist stress inside the coating body [28], thus expanding the blistering time of the coatings and the time interval. For example, in Fig. 10 and Table 4, sample 7 and 8 have better adhesion and greater the time interval. The above results show that the use of the EFT can significantly shorten the test time. Note that in this experiment, the defined EFT depends on the appearance of the diffusion arc at the low frequency region in the impedance diagrams due to the effects of corrosion products. However, it may not be suitable for other anticorrosive coatings with sacrificial-to-barrier protection mechanism since the second arc appears in the impedance spectrum at the early stage [29], which enables us to redefine the electrochemical failure time, taking the specific failure mechanism into consideration. More work about waterborne coatings with other pigments is in progress.

As we know, some electrochemical parameters have been proposed to evaluate the properties of coatings, such as f_b, ϕ_{10Hz}, etc. But for a specific coating, whether these methods have a consistent conclusion has not been validated. In this paper, the conclusions summarized by these methods for quickly evaluating the performance of the waterborne epoxy coatings prepared were confirmed to be consistent. Furthermore, the concept of the EFT is put forward for the first time. It is a combination of the failure mechanism of a specific coating and its Nyquist diagrams. We define the EFT based on the obvious changes of curve in Nyquist diagrams due to the effects of the corrosion products. Moreover, it corresponds to the failure time in conventional corrosion tests, indicating there exist more practical

links between EIS and conventional corrosion tests. Historically, the focus of associating the EIS with conventional corrosion tests was to establish a link between the rank based on impedance data and the classification determined visually [8].

4. CONCLUSIONS

- The good comprehensive performance of the paint is obtained when the 600-mesh-sized MIO is used and the PVC is 39% by EIS and general performance test.
- The electrochemical behavior of waterborne epoxy micaceous iron oxide paint shows that the coating resistance first decreases rapidly, and then declines slowly until the coating failed. The two methods for quickly evaluating properties of coatings are consistent, reflecting both the changes of coatings performance and their relationship with coating properties. Both the variations of the partial fitting coating resistance and the phase angle at 10 Hz are almost identical with the variation of the coating resistance. The decrease of R_{part} to 10^6 $\Omega \cdot cm^2$ and the decline of $\boldsymbol{\phi}_{10Hz}$ to the range of $10°$-$20°$ indicate the strong corrosion reactions occur in the steel/coating interface and the diffusion behaves obviously.
- Using the defined EFT can obviously shorten the conventional corrosion test cycle, which is expected to be used in product development. Improving the adhesion of coatings on steel substrates may enhance the ability to resist the stress inside the coatings body, thereby extending the time interval and drastically shortening the characterization time compared with the conventional corrosion test.

References

1. Y. F. Zhu, J. P. Xiong, Y. M. Tang, and Y. Zuo. *Prog. Org. Coat.*, 69 (2010) 7.
2. Y. Cubides and H. Castaneda. *Corros. Sci.*, 109 (2016) 145.
3. S. Skale, V. Dolecek and M. Slemnik, *Prog. Org. Coat.*, 62 (2008) 387.
4. X.M. Li, B. Faber, B. Minch and H. Castaneda, *Corrosion*, 70 (2014) 615.
5. M. Mahdavian and M. M. Attar, *Corros Sci.*, 48 (2006) 4152.
6. I. Sekine, K. Sakaguchi and M. Yuasa, *J. Coat. Technol.*, 45 (1992) 64.
7. F. Mansfeld. *J. Appl. Electrochem.*, 25 (1995) 187.
8. F. Mansfeld and C. H. Tsai, *Corrosion*, 49 (1991) 958.
9. A. T. Xu, F. Zhang and F. Jin, *Int. J. Electrochem. Sci.*, 9 (2014) 5116.
10. X Li and H Castaneda, *Corros. Eng. Sci. Techn.*, 50 (2015) 218.
11. C. N. Su, W. Wu, Z. P. Li and Y. Guo, *Corros. Sci.*, 99 (2015) 42.
12. F. Mahdavi, Mike Y.J. Tan and M. Forsyth, *Prog. Org. Coat.*, 88 (2015) 23.
13. C. Yu, P. Wang and X. H. Gao, *Int. J. Electrochem. Sci.*, 10 (2015) 538.
14. E. Akbarinezhad, M. Bahremandi, H. R. Faridi and F. Rezaei, *Corros. Sci.*51 (2009) 356.
15. Y. Zuo, R. Pang, W. Li, J. P. Xiong and Y. M. Tang, *Corros. Sci.*, 50 (2008) 3322.
16. L. Liang, J. M. Hu, J. Q. Zhang and C. N. Cao, *Corros. Sci. Prot. Techn.*, 22 (2010) 325.

17. Y. J. Zheng, Z. C. Liu, *Powder Technol.*, 207 (2011) 335.
18. P. Kalenda, A. Kalendová, V. Štengl, P. Antoš, J. Šubrt, Z. Kváa, S. Bakardjieva, *Prog. Org. Coat.*, 49 (2004) 137.
19. B. Nikravesh, B. Ramezanzadeh, A. A. Sarabi and S. M. Kasiriha, *Corros. Sci.*, 53 (2011) 1592.
20. A. Kalendová, D. Vesely, I. Sapurina and J. Stejskai, *Prog. Org. Coat.*, 63 (2008) 228.
21. J. M. Hu, J. T. Zhang, J. Q. Zhang and C. N. Cao, *Corros. Sci.*, 47 (2005) 2607.
22. J. B. Bajat, I. Milošev, Ž. Jovanović and V. B. Mišković-Stanković, *Appl. Surf. Sci.*, 256 (2010) 3508.
23. P. Calvez, S. Bistac, M. Brogly, J. Richard and D. Verchere, *J. Adhesion*, 22 (2012) 145.
24. T. Prosek, A. Nazarov, M. G. Olivier, C. Vandermiers, D. Koberg and D. Thierry, *Prog. Org. Coat.*, 68 (2010) 328.
25. Y. L. Huang, X. M. Yu and W. J. Qu, *Int. J. Electrochem. Sci.*, 9 (2014) 185.
26. C. H. Hare, *J. Prot. Coat. Lin.*, 3 (1998) 17.
27. K. R. Gowers and J. D. Scantlebury, *Corros. Sci.*, 23 (1983) 935.
28. P. Araujo, D. Chicot, M. Staia, and J. Lesage, *Surf. Eng.* 21 (2005) 35.
29. K. Schaefer, and A. Miszczyk, *Corros. Sci.*, 66 (2013) 380.